ISSN 1023-1935, Russian Journal of Electrochemistry, 2018, Vol. 54, No. 11, pp. 825–834. © Pleiades Publishing, Ltd., 2018.
Original Russian Text © A.G. Krivenko, R.A. Manzhos, N.S. Komarova, A.S. Kotkin, E.N. Kabachkov, Yu.M. Shul'ga, 2018, published in Elektrokhimiya, 2018, Vol. 54, No. 8S, pp. S32–S41.

Comparative Study of Graphite and the Products of Its Electrochemical Exfoliation

A. G. Krivenko[a], R. A. Manzhos[a], *, N. S. Komarova[a], A. S. Kotkin[a], E. N. Kabachkov[a], and Yu. M. Shul'ga[a]

[a] *Institute of Problems of Chemical Physics, Russian Academy of Sciences, Chernogolovka, Moscow oblast, 142432 Russia*
**e-mail: rmanzhos@icp.ac.ru*

Received July 14, 2017; in final form, December 29, 2017

Abstract—A comparative study of electrochemical characteristics of graphite electrodes and precipitates of suspensions produced by the graphite exfoliation is carried out. The graphite is exfoliated into low-layered graphene structures formed in the course of electrochemical impact during the applying of alternating potential to the electrodes. The low-layered graphene structures and graphite electrodes were characterized using numerous procedures from optical, electron, and scanning microscopy, UV-vis-, IR-, Raman, and XPS-spectroscopy, and thermogravimetric analysis. The rate constant of electron transfer at the initial graphite for $[Ru(NH_3)_6]^{2+/3+}$ and $[Fe(CN)_6]^{4-/3-}$ redox pairs is shown to approach the value measured both for the low-layered graphene structures obtained during the graphite electrode exfoliation and for highly oriented carbon nanowalls and single-walled nanotubes measured earlier. At the same time, the $Fe^{2+/3+}$ redox-process occurring at the graphite electrode is faster than at the low-layered graphene structures and much faster (by 2–3 orders of magnitude) than at the nanowalls. It is concluded that no significant acceleration of the electron transfer generally occurs when passing from the graphite electrodes to the low-layered graphene structures.

Keywords: graphite, exfoliation, electron transfer, redox-reactions, low-layered graphene structures, $[Ru(NH_3)_6]^{2+/3+}$, $[Fe(CN)_6]^{4-/3-}$, $Fe^{2+/3+}$

DOI: 10.1134/S1023193518110058

INTRODUCTION

It is current opinion nowadays that carbon nanostructured isomorphs are the basis for the production of perspective electrodes with outstanding electrocatalytic properties [1–3]. At the same time, the using of manifold industrially produced graphites as electrodes is undoubtedly difficult because of their destruction (crumbling) at high current densities. The development of new, more effective materials is required. Electrodes based on different carbon nanoforms are considered as the candidates. They are as follows: fine-dispersed carbon blacks, fullerenes, nanotubes, manifold graphene-like structures, and the combination thereof. As to the latter ones, their preparation methods are also miscellaneous, varying from traditional chemical and CVD-deposition and up to hydromechanical detachment and laser or microwave heating [4–6]. A trend in the field is the graphite electrochemical exfoliation that allows producing suspensions of low-layered graphene structures in organic and inorganic electrolytes in a simple and effective way. It is believed that the low-layered graphene structure detachment from graphite surface under the applying of cathodic potential is mainly caused by the electrolyte anions or cations intercalation to interplanar space, followed by formation of covalent or ionic bonds. This eventually leads to the detachment of graphene-like particles from the "continental" electrode [7]. In some published papers describing the electrochemical exfoliation of graphite attached to the glassy carbon substrate the key role of the intercalation in the process was also suggested [8, 9]. The adding of strong surfactants to the solutions [10] often facilitates the process. Some authors believe that the electrochemical exfoliation mechanism actually is more complicated than mere loosening of the surface layer. The key role in its first stage is played by active intermediates (radicals and radical-ions) formed at the water electrolysis, that functionalize the graphite edge and thus attenuate Van der Waals forces between the basal planes, hence, facilitate the anion intercalation to the interplanar space [11, 12]. As to the surface functionalization level of the low-layered graphenes formed during the electrochemical action, the literature data well varied. In particular, relatively low oxygen content (6.5 and 4.1 at %, respectively) was regis-

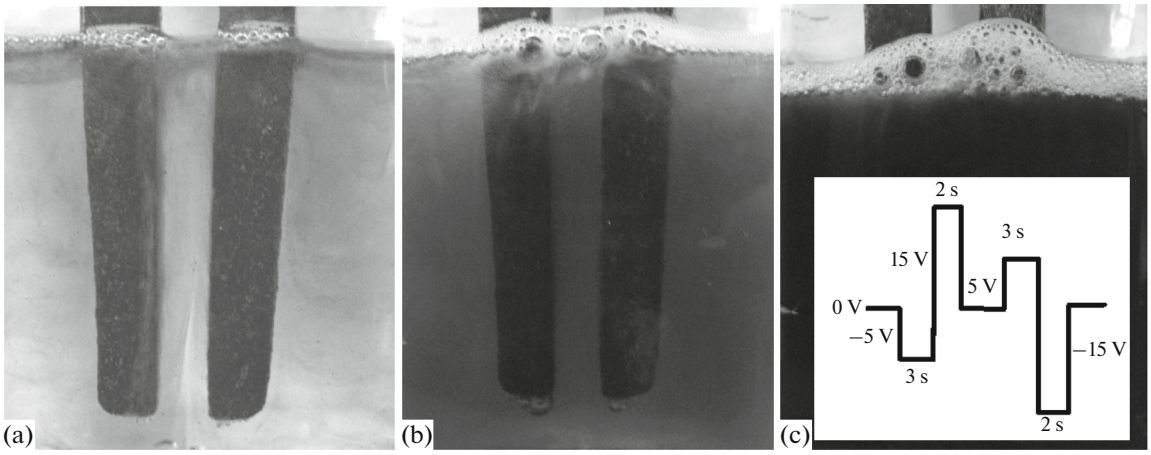

Fig. 1. Photographs of the cell with graphite electrodes, taken after different times of electrochemical impact: (a) 30 s, (b) 20 min, (c) 40 min. Insert: time diagram of the applied voltage.

tered at the low-layered-graphenes' surfaces in works [13] and [14], whereas in work [11] much larger oxygen content (~29 at %) was detected. At that, particular methods of the electrode preparation differ significantly. According to the authors [11], these facts point to wide potentialities of the controlling of the low-layered graphene surface functionalization degree in the course of electrochemical impact.

Our analysis of literature showed that the studying of electrocatalytic properties of the carbon nanoforms (in particular, the low-layered carbon structures) generally comprises a few of sequential stages. Firstly, the graphite is split, most often using a method similar to that suggested by Hummers [15], thus giving an oxidized nanoform suspension. Then, the nanoforms are deposited onto a conducting support surface, with subsequent reduction, even if partial, of the deposit. Lastly, proper electrochemical measurements are performed, aiming at a revelation of the catalytic activity [16, 17]. A simpler, green approach based on the carbon isomorph obtaining and studying in the context of purely electrochemical procedures is much more rarely used. However, in the works where the low-layered graphene dispersions were obtained by the graphite electrochemical exfoliation most often no comparative study of the electron transfer rate on the prepared deposits in comparison with graphite electrode and other carbon nanoforms was carried out [18]. In this work, we suggest the testing of electrochemical characteristics of the low-layered graphene deposits prepared by the graphite electrode pulsed electrochemical processing, together with the testing of the graphite electrode itself. As the criteria for such a comparison, results of the characterizing of the low-layered graphene structure deposits and the graphite electrode with different physical methods, as well as kinetic parameters of model redox reactions, are used.

EXPERIMENTAL

Experiments with the graphite exfoliation were performed in a two-electrode glass cell, in 0.1 M Na_2SO_4 aqueous solution. The electrodes were two identical GR-280 graphite rods with the cross-section of ~10 × 10 mm and the length of ~5–10 cm. The electrode polarization and the current control in the system were carried out using a computerized P-150S high-current potentiostat (Elins, Russia). The electrodes were exposed to repetitive cycles of anodic—cathodic voltage pulses with the following time diagram: 5 V 3 s, −15 V 2 s, −5 V 3 s, 15 V 2 s (Fig. 1). The pulse rise time at the electrode was 1–5 ms. The electrolysis time varied from 1 to 10 h. Upon completion of the graphite electrochemical exfoliation, the suspension formed was kept for ~12 h; as a result, the low-layered graphenes mainly precipitated to a loose deposit, and the solution somewhat decolorized. The solution was neatly decanted; the rest of it was diluted with distilled water. Upon the re-precipitation, the solution was decanted repeatedly. With the decreasing of salt concentration in the solution, the suspension became increasingly stable; practically no precipitation occurred. On this reason, its centrifuging at 5500 rpm (~8000 *g*) was performed for the low-layered graphene structure further washing from traces of the electrolyte. Upon separation of the aqueous solution in the centrifuge, the precipitate was added with distilled water, and two more centrifuging cycles were carried out. As a result, we obtained stable low-layered graphene structure suspension with the concentration of 1.0–10 mg/mL; it was then sonicated for 10–20 min and put to a glass beaker. To perform electrochemical measurements, controlled amount of suspension with known low-layered graphene structure concentration was applied to glassy carbon surface and kept to the complete drying. Voltammograms of the graphite

electrodes were taken at the initial-graphite rods (with the cross-section of ~0.5 cm^2) partly plunged into the solution. Besides, control measurements were carried out with the graphite electrodes assembled in the same way as electrodes with low-layered graphene deposits. The electrodes were prepared by the applying of aqueous suspension of mechanically grinded initial graphite, with minor addition of Nafion (2 wt %), to glassy carbon electrode.

The graphite and low-layered graphene structure electrodes were characterized using a Carl Zeiss Supra 40 system scanning electron microscope with an INCA Energy X-ray energy-dispersive spectrometer. IR-spectra were recorded using an "Alpha" FTIR spectrometer (Brucker); the samples were KBr tablets with the pressed-in low-layered graphene structures. UV-vis-NIR-spectra of the low-layered graphene structure suspensions were recorded using a SPECS-SSP-705-1 spectrometer. Raman spectra were recorded using a Renishaw InVia Reflex spectrometer with laser excitation at a wavelength of 976 nm (power 30 mW). XPS-spectra were obtained using a Specs instrument (Germany), with a Phoibos 150 semispherical analyzer with MgK_α-radiation (1253.6 eV). The pressure in the spectrometer work chamber did not exceed 5×10^{-8} Pa.

Cyclic voltammograms were recorded using a P-30S potentiostat (Elins, Russia) in a three-electrode system. A quartz cell was used. Aqueous 1 M Na_2SO_4 solution was the supporting electrolyte in all cases except $FeSO_4$ solutions. The $[Ru(NH_3)_6]Cl_3$, $K_3[Fe(CN)_6]$, and $FeSO_4 \cdot 7H_2O$ chemicals were used as received; their concentration was 5 mM. Twice-distilled (in quartz vessel) water was used for the solution preparation. All potentials are referenced to saturated calomel electrode (SCE).

RESULTS AND DISCUSSION

The imposition of the voltage pulses induced intense gas (hydrogen and oxygen) evolution, accompanied by the graphite exfoliation and the formation of aqueous suspension of the electrode exfoliation products (Fig. 1). In Fig. 2 we show SEM-microphotographs of the graphite and low-layered graphene structure surfaces. Crumpled surface, relatively smooth on a micrometer scale (Fig. 2a), is typical of the initial graphite whereas the low-layered graphene structures represent graphene-like laciniate particles with wide distribution in their lateral size (the estimated half-width lies in the 200–600 nm range). The SEM-microphotograph-based graphene-like structure thickness was estimated being 2–4 nm. In Fig. 3a we give Raman spectra for the low-layered graphene structure aqueous suspension recorded with the excitation light wavelength of 976 nm. In compliance with

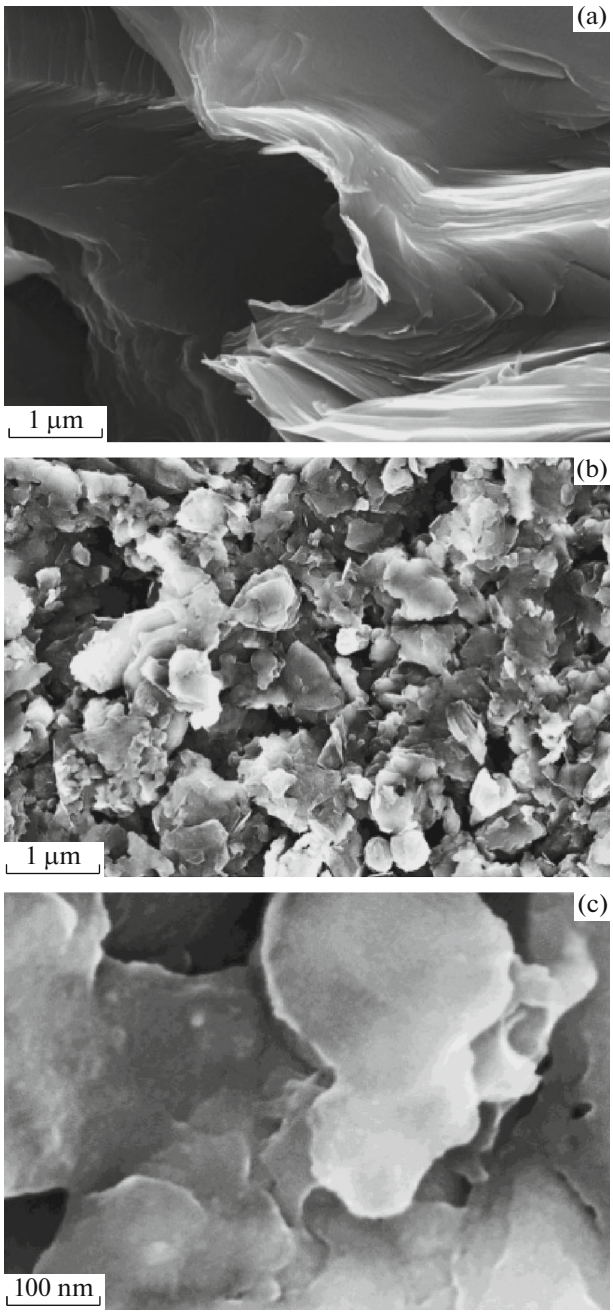

Fig. 2. SEM-microphotographs of (a) graphite surface and (b), (c) low-layered graphene structure precipitate.

the data [1], the spectrum appearance corresponds to lightly imperfect low-layered graphene structures. Indeed, the G/D line intensity ratio is ~3, whereas the broad 2D line is shifted toward lower wave numbers as compared with the graphite. The most intensive absorption bands in the IR-spectra of the low-layered graphene structures (Fig. 3b) are observed near 1720 cm^{-1}, which corresponds to the C=O bond vibrations in carboxyl groups, and at ~3300–3500 cm^{-1},

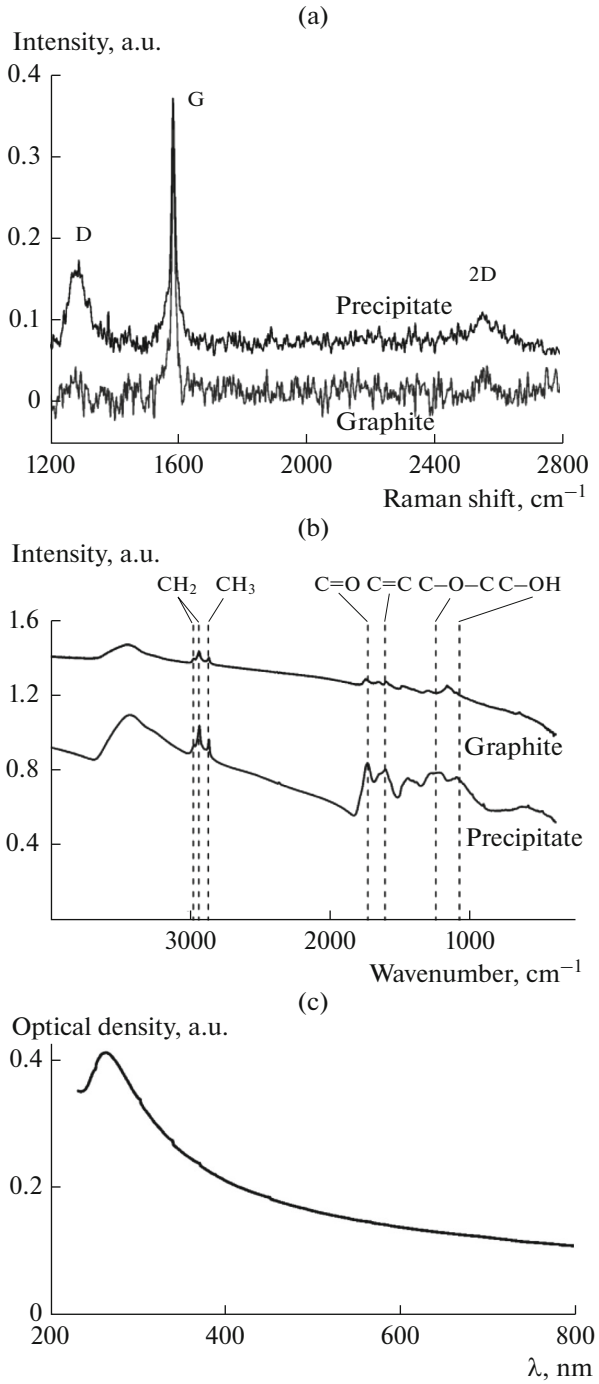

Fig. 3. Raman (a) and IR-absorption spectra (b) of graphite and low-layered graphene structure precipitate; (c) UV-vis-NIR-spectrum of aqueous suspension of low-layered graphene structure.

which can be attributed to the C–OH and C–OOH bond vibrations, that is, to hydroxyl and carboxyl groups. Besides, the low-layered graphene structure samples contain CH_2-fragments or methylene groups, because absorption bands at 2923 and 2855 cm^{-1} are observed, as well as CH_3-groups (2963 cm^{-1}), see, e.g., work [19]. Practically the same absorption bands are characteristic of graphite; however, they are much weaker pronounced. In Fig. 3c we show UV-vis-NIR-spectrum of the low-layered graphene structure aqueous suspension; it demonstrates distinct features typical of the low-layered graphene spectroscopy: a maximum at $\lambda \approx 270$ nm and rather high absorption of visible light [20, 21]. According to elemental and thermogravimetric analysis, the oxygen bulk concentration in the low-layered graphene structure and graphite electrode powders is ~2–3 and ~1 at %, respectively. The quantitative and qualitative determination of the oxygen-containing groups at the low-layered graphene structure and initial graphite electrodes' surfaces was carried out by the XPS method. In Fig. 4a we give C1*s* XPS-spectra of the initial graphite and the precipitate of the low-layered graphene structure suspension obtained in the course of the graphite exfoliation, normalized with respect to the peak intensity. We see that the studied samples' spectra differ from the reference spectrum only in their larger half-width and higher spectrum intensity at the side of higher binding energy of the main maximum. In order to determine the possible contribution to the experimental spectrum from the carbon atoms of the functional groups, we resolved all spectra into mixed Gauss–Lorenz components, upon the background subtraction according to Shirley [22]; for the most intensive peak ascribed to carbon atoms not bound to the functional groups, we introduced an asymmetry parameter. Our analysis of different variants of the resolving showed that the most realistic is the using, in addition to the peak at 284.8 eV (C–C), of four mixed components shifted relatively to the main peak by +1.4 (C–OH), +2.1 (C–O–C), +3.0 (C=O), and +4.2 (O–C=O) eV. The functional group assignment was carried out in compliance with the work of reference [23]. An example of the suspension spectrum resolving into five components is shown in Fig. 4b. It demonstrates reasonable agreement between the calculated and experimental curves. In Table 1 we present (in atomic percent) the percentage of the functional groups determined from the intensities of the corresponding peak obtained by the resolving of the spectra of studied samples into five components [24].

We see from Table 1 that all functional groups other than carboxyl ones are present at the graphite surface; whereas at the low-layered graphene structure surfaces the carboxyl groups appeared and the other group concentration increased.

The above-given data on the graphite- and the low-layered-graphene-structure-based electrodes' characterization points to some degree of similarity in the objects' morphology and functionalization. On this reason, it is advisable to carry out a comparative study

of electrochemical characteristics of initial graphite and the electrodes on the base of the low-layered graphene structure precipitates synthesized by electrochemical method. The capacitance of the latter electrodes determined from the cyclic voltammograms obtained in solutions containing no redox systems exceeded the analogous quantity for the glassy carbon by a factor of 40–50: it was about 50–70 F/g. The obtained value is close to the data found for both morphologically similar graphene-like structure precipitates [25, 26] and electrodes based on single-walled carbon nanotubes [27–29] and highly oriented carbon nanowalls [30], differing significantly with respect to their surfaces' structure. When we assume the quantity of ~20 μF/cm^2 as a specific capacitance of graphene sheet in aqueous electrolyte solution [31] and 2630 m^2/g as a limit surface area of the two-sided graphene sheet, then the low-layered graphene structure mean thickness equals to ~10 basal planes, or ~3.5 nm; and this corresponds to the above-given estimate.

We used abundant redox systems $[Ru(NH_3)_6]^{2+/3+}$, $[Fe(CN)_6]^{4-/3-}$, and $Fe^{2+/3+}$ as testing reactions. They differ significantly both in the sensitivity of the electron transfer rate constant k^0 with respect to the surface state and in their equilibrium potentials E^*. The system $[Ru(NH_3)_6]^{2+/3+}$ is thought of as the nearest to an ideally outer-sphere one, hence, low-sensitive to the electrode surface state. By contrast, the system $Fe^{2+/3+}$ is considered as the most sensitive to the surface state, whereas the redox pair $[Fe(CN)_6]^{4-/3-}$ is an intermediate. We compared the redox-system kinetic characteristics by analyzing the dependences of the potential difference between the anodic and cathodic current peaks (the peak separation, ΔE) in the cyclic voltammograms on the potential scan rate v, that varied over wide (3–500 mV/s) range. Typical cyclic voltammograms are shown in Fig. 5. It should be noted that the above-listed redox-systems gave symmetrical, nearly linear dependences of the anodic and cathodic peak currents on $v^{0.5}$, whose extrapolated curves crossed the origin. No effect of the cycle number on the voltammogram shape was observed at the studied electrodes.

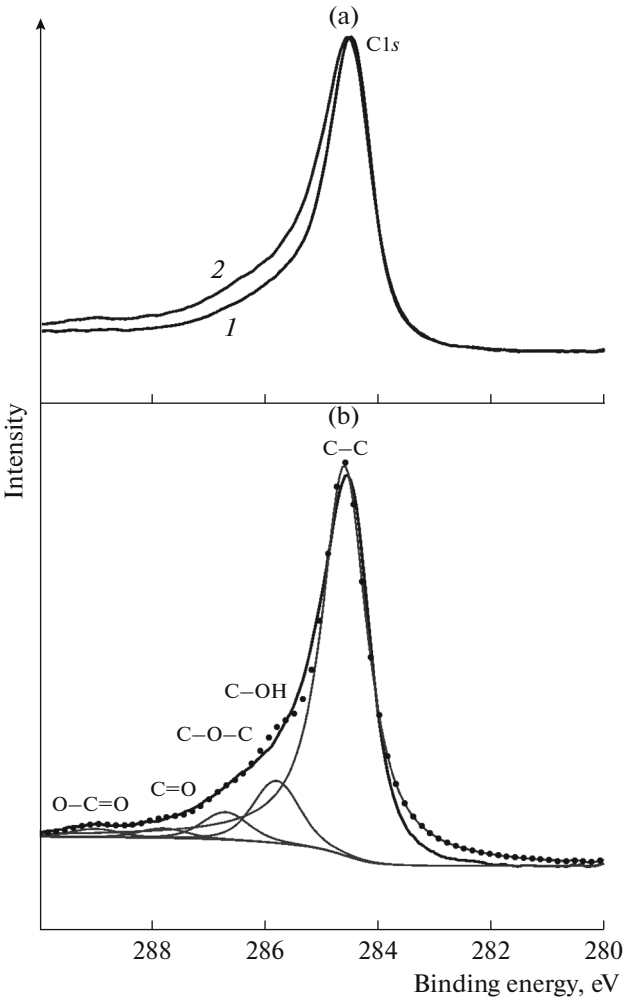

Fig. 4. (a) High-resolution C1s spectra of initial graphite (*1*) and precipitate of suspension (*2*); (b) decomposition of C1*s* spectrum of deposited suspension (points) into 5 components. The functional group assignment is denoted in the figure.

As a rule, we evaluated the electron transfer rate constants k^0 at the potential $E = E^*$ by comparing the calculated and experimental dependences $\Delta E(v)$ in the diffusion, mixed diffusion-kinetic, and kinetic regions of the passed redox-process. In other words, we varied v as wide as possible, in order to cover the

Table 1. Decomposition parameters for C1*s* spectra of graphite and low-layered graphene structure precipitates

Sample	C–C (at %)	C–OH (at %)	C–O–C (at %)	C=O (at %)	O–C=O (at %)
Graphite	86.6	7.5	3.7	1.1	0
Precipitate	82.9	9.9	4.4	1.5	1.3

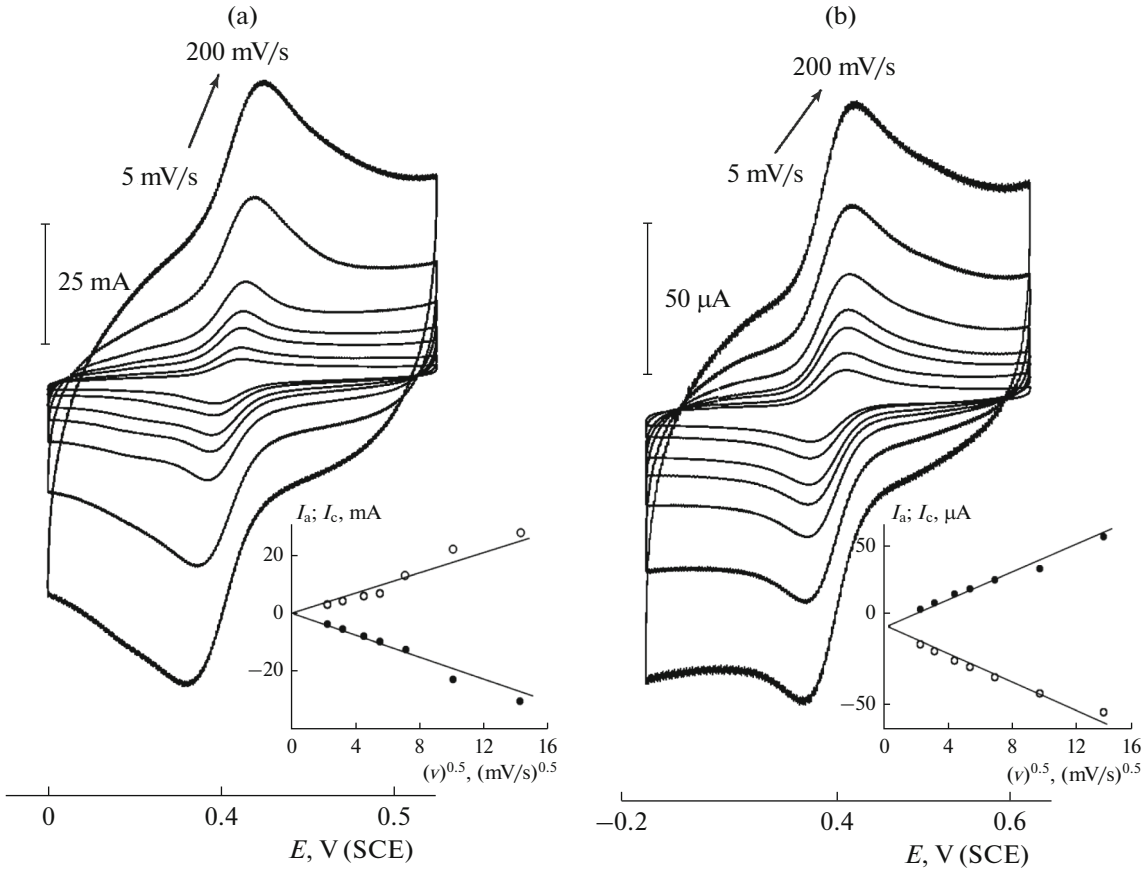

Fig. 5. Typical recorded cyclic voltammograms: (a) graphite electrode in 0.1 M Na_2SO_4 + 0.005 M $FeSO_4$ + 0.25 M H_2SO_4 solution; (b) low-layered graphene structure suspension in 1 M Na_2SO_4 + 0.005 M $K_3[Fe(CN)_6]$ solution. Inserts: dependences of maximum currents of anodic (I_a) and cathodic (I_c) peaks on $(v)^{0.5}$ for $Fe^{2+/3+}$ and $[Fe(CN)_6]^{4-/3-}$ redox-reactions, respectively.

transition from the region where ΔE approached the thermodynamic value of 59 mV and did not depend on v to the kinetic region where ΔE is proportional to log$v$. The calculated cyclic voltammograms were obtained using the formulas given in work [32]. We assumed the diffusion coefficient being 10^{-5} cm^2/s for all reactants; the redox-reaction transfer coefficient, 0.5. Earlier we showed that the error in the k^0 determination caused by the decreasing of the diffusion coefficient by a factor of 2, as well as by the varying of the transfer coefficient over the range of 0.6–0.4, does not exceed that caused both by the spread of experimental points and the discordance between the real topology of the nanostructured surface and the idealized one underlying our simulation model [30].

In Fig. 6 we give experimental dependences of the peak separation in the cyclic voltammograms on the potential scan rate for the test redox-systems at the low-layered graphene structures and the graphite electrodes. For the comparison sake, we also showed similar data for the electrodes based on the highly oriented carbon nanowalls [33]. It is evident, from the comparison of experimental dependences with the calculated ones, that the effect of the electrode nature on the electron transfer rate in the different redox-systems is alternate. In the case of $[Ru(NH_3)_6]^{2+/3+}$, the k^0 values for the low-layered graphene structures and nanowalls practically coincided ($k^0 \approx 5 \times 10^{-2}$ cm/s), whereas for the graphite electrode the electron transfer rate is somewhat less (by a factor of 2–3). Similar situation occurs for $[Fe(CN)_6]^{4-/3-}$, with the only difference that the value of $k^0 \approx 5 \times 10^{-3}$ cm/s coincided for the low-layered graphene structures and the graphite electrodes, whereas the electron transfer rate at the carbon nanowalls is higher by the same factor of 2–3. The obtained results for the studied redox-systems are in good compliance with the literature data obtained for single-walled carbon nanotubes, basal plane edges of HOPG (see, e.g., [34, 35]), and the amorphous graphite and thermally reduced graphene oxide precipitates [36]. The coincidence is hardly occasional; it points out to the similarity of conditions for the elec-

tron transfer at the electrodes so differing in their surface morphology. It should be noted that the comment [37] on the possible inaccuracy in the measured k^0 values caused by the effective porosity of the low-layered graphene structure precipitates and the initial graphite is not relevant in the case of the carbon nanowalls because of their quite sufficient accessibility for electrolyte solution [38]. The situation is likely to be characteristic of the carbon nanotubes as well [34]. Moreover, the likeness of the k^0 values cannot be explained by mere insensibility of the electron transfer rate in the redox-systems to surface morphology because the values k^0 of these reactions measured at basal planes and at the plane edges differ significantly [39, 40]. Thus, it can be concluded that the outer-sphere electron transfer rates for the electrodes based on the carbon nanoforms and commercial graphite practically coincide.

Quite different situation is characteristic of the $Fe^{2+/3+}$ redox-system. In this case, the electron transfer rate constant is maximal for the graphite electrode, much less for the low-layered graphene structures, and by 2–3 orders of magnitude less for the initial carbon-nanowall-based electrode. This result must be thought of as well expectable because the $Fe^{2+/3+}$-reaction is rather sensitive to the amount of oxygen at the electrode surface According to the XPS-spectroscopy data, the amount of oxygen-containing functional groups at the graphite electrode surface is much larger than at the initial carbon nanowall surface. As to the k^0 ratio for the graphite- and low-layered-graphene-structure-electrodes, a possible reason for the decreased electron transfer rate at the latter is the formation of quinone groups at the low-layered graphene structure surfaces, which manifest themselves most clearly in the redox-system-free acid solutions. One can suggest that the presence of these groups will block in part the redox-process. This suggestion is substantiated by the observation of the anodic-cathodic current peaks in the cyclic voltammograms at anodic potentials, with the formal potential $E^* \approx 0.3$–0.4 V. At that, unlike the redox-systems, the ΔE value for the peaks is significantly less than 58 mV; it is independent of the potential scan rate at $v \le 100$ mV/s, whereas the peak amplitude grows linearly with the increasing of v (Fig. 7). These characteristics correspond to the data published recently [41]; in the quoted work the presence of the quinone groups at the surface of different graphite electrodes was proved unambiguously. Detailed study of the quinone group formation at the surface of electrochemically synthesized low-layered graphene structures will be the topic of future work.

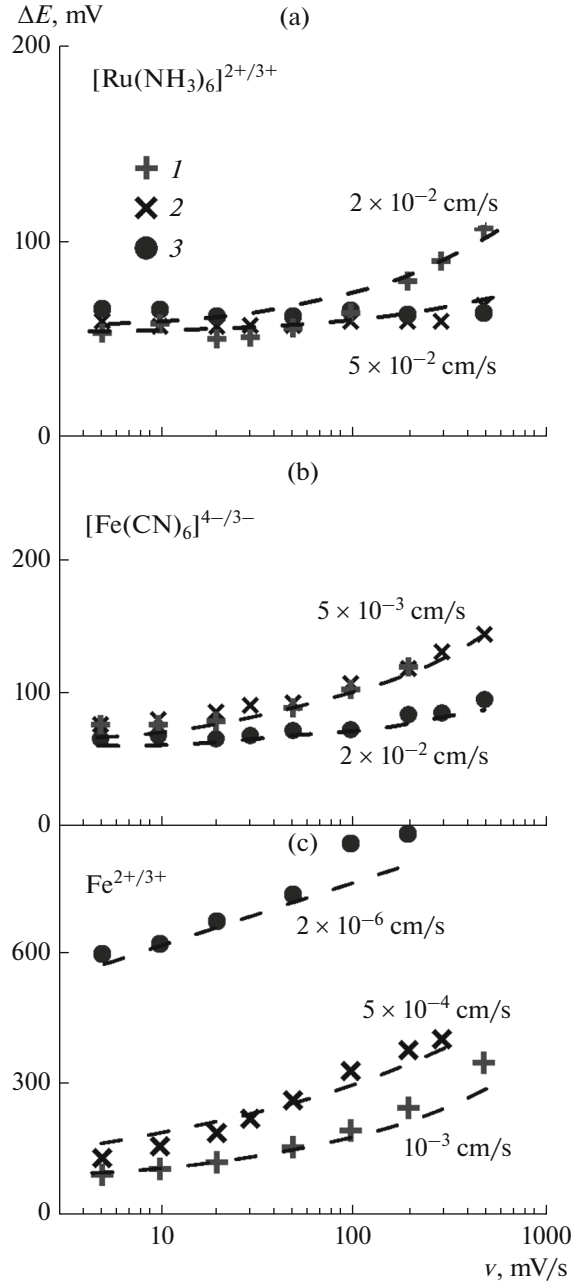

Fig. 6. Dependence of peak separation on potential scan rate for the redox-systems: (a) $[Ru(NH_3)_6]^{2+/3+}$, (b) $[Fe(CN)_6]^{4-/3-}$; (c) $Fe^{2+/3+}$: (*1*) graphite, (*2*) low-layered graphene structure precipitate, (*3*) dependences $\Delta E(v)$ for carbon nanowalls (data of [33]). Dashed lines—calculated $\Delta E(v)$ dependences for k^0 values shown near the curves.

CONCLUSIONS

The analysis of data obtained in the comparative study of the $[Ru(NH_3)_6]^{2+/3+}$, $[Fe(CN)_6]^{4-/3-}$, and $Fe^{2+/3+}$ redox-systems at the initial graphite and low-

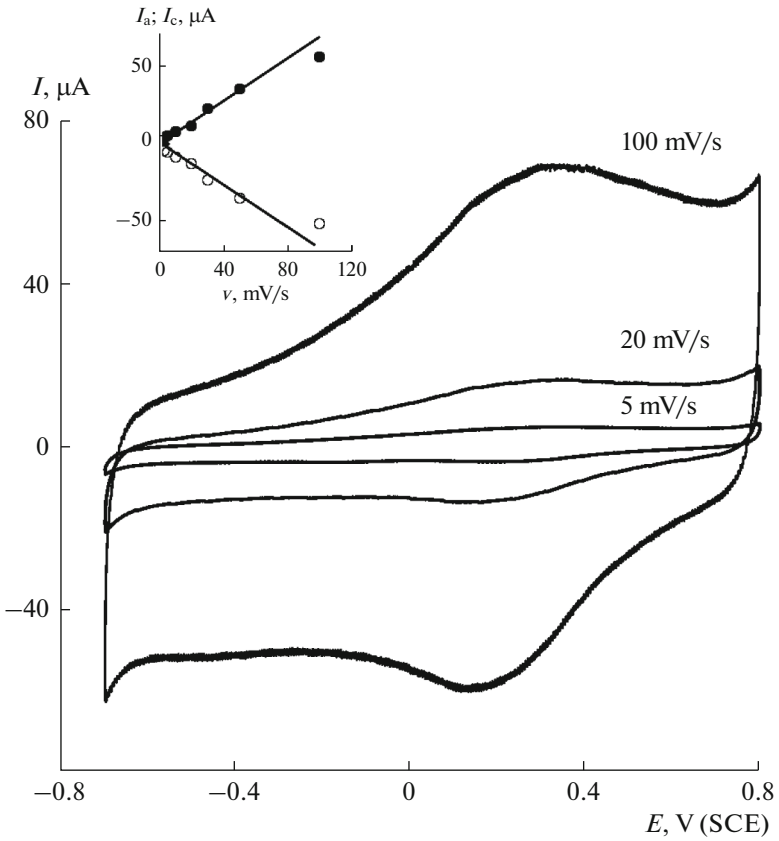

Fig. 7. Typical cyclic voltammograms recorded in solution 0.1 M Na_2SO_4 + 0.1 M H_2SO_4. Insert: dependences of maximum currents of anodic (I_a) and cathodic (I_c) peaks on *v*.

layered graphene structure precipitates prepared by the graphite electrochemical exfoliation showed that the k^0 values for the first two reactions are close to each other. Thus, the data obtained in this work point to the absence of an a priori significant increase in the electrocatalytic activity for the particular electrode processes when passing from graphite electrode to those based on low-layered graphene structure precipitates or other carbon nanoforms.

ACKNOWLEDGMENTS

This work was supported by the Russian Foundation for Basic Research, project no. 16-03-00475a.

REFERENCES

1. Kannan, M.V. and Kumar, G.G., Current status, key challenges and its solutions in the design and development of graphene based ORR catalysts for the microbial fuel cell applications, *Biosensors Bioelectronics*, 2016, vol. 77, p. 1208.
2. Chua, C.K. and Pumera, M., Carbocatalysis: The State of "Metal-Free" Catalysis, *Chemistry-European J.*, 2015, vol. 21, p. 12550.
3. Kamiya, K., Hashimoto, K., and Nakanishi, S., Graphene Defects as Active Catalytic Sites that are Superior to Platinum Catalysts in Electrochemical Nitrate Reduction, *ChemElectroChem.*, 2014, vol. 1, p. 858.
4. Shinde, D.B., Brenker, J., Easton, C.D., Tabor, R.F., Neild, A., and Majumder, M., Shear Assisted Electrochemical Exfoliation of Graphite to Graphene, *Langmuir*, vol. 32, p. 3552.
5. Strong, V., Dubin, S., El-Kady, M.F., Lech, A., Wang, Y., Weiller, B.H., and Kaner, R.B., Patterning and Electronic Tuning of Laser Scribed Graphene for Flexible All-Carbon Devices, *ACS NANO*, 2012, vol. 6, p. 1395.
6. Shulga, Y.M., Baskakov, S.A., Knerelman, E.I., Daidova, G.I., Badamshina, E.R., Shulga, N.Yu., Skryleva, E.A., Agapov, A.L., Voylov, D.N., Sokolov, A.P., and Martynenko, V.M., Carbon nanomaterial produced by microwave exfoliation of graphite oxide: new insights, *RSC Advances*, 2014, vol. 4, p. 587.
7. Disa, N. Md., Bakar, S.A., Alfarisa, S., Mohamed, A., Isa, I. Md., Kamari, A., Hashim, N., and Mahmood, M.R., A Review: Synthesis Methods of Graphene and Its Application in Supercapacitor Devices, *Advantage Mater. Res.*, 2015, vol. 1109, p. 40.
8. Simonet, J., Electrochemical exfoliation in real time of natural graphite deposited onto glassy carbon. Doping

and modifying carbons through ultra-thin graphite layers, *Electrochem. Commun.*, 2014, vol. 48, p. 142.

9. Jouikov, V. and Simonet, J., Graphene: Large Scale Chemical Functionalization By Cathodic Means, *Electrochem. Commun.*, 2014, vol. 46, p. 132.
10. Alanyalıoglu, M., Segura, J.J., Oro-Sole, J., and Casan-Pastor, N., The synthesis of graphene sheets with controlled thickness and order using surfactant-assisted electrochemical processes, *Carbon*, 2012, vol. 50, p. 142.
11. Zeng, F., Sun, Z., Sang, X., Diamond, D., Lau, K.T., Liu, X., and Su, D.S., In Situ One-Step Electrochemical Preparation of Graphene Oxide Nanosheet-Modified Electrodes for Biosensors, *ChemSusChem*, 2011, vol. 4, p. 1587.
12. Rao, K.S., Senthilnathan, J., Liu, Y.-F., and Yoshimura, M., Role of Peroxide Ions in Formation of Graphene Nanosheets by Electrochemical Exfoliation of Graphite, *Sci. Reports*, 2014, vol. 4, p. 4237.
13. Ejigu, A., Kinloch, I.A., and Dryfe, R.A.W., Single Stage Simultaneous Electrochemical Exfoliation and Functionalization of Graphene, *ACS Appl. Mater. Interfaces*, 2017, vol. 9, p. 710.
14. Yen, P-J., Ting, C-C., Chiu, Y.-C., Tseng, T.-Y., Hsu, Y.-J., Wua, W.-W., and Wei, K.-H., Facile production of graphene nanosheets comprising nitrogen-doping through in situ cathodic plasma formation during electrochemical exfoliation, *J. Mater. Chem. C*, 2017, vol. 5, p. 2597.
15. Hummers, W.S. and Offeman, R.E., Preparation of Graphitic Oxide, *J. Am. Chem. Soc.*, 1958, vol. 80, p. 1339.
16. Javed, S.I. and Hussain, Z., Covalently Functionalized Graphene Oxideq—Characterization and Its Electrochemical Performance, *Int. J. Electrochem. Sci.*, 2015, vol. 10, p. 9475.
17. Wu, F., Huang, T., Hu, Y.J., Yang, X., Ouyang, Y.J., and Xie, Q.J., Differential pulse voltammetric simultaneous determination of ascorbic acid, dopamine and uric acid on a glassy carbon electrode modified with electroreduced graphene oxide and imidazolium groups, *Microchim. Acta*, 2016, vol. 183, p. 2539.
18. Parvez, K., Wu, Z.-S., Li, R., Liu, X., Graf, R., Feng, X., and Müllen, K., Exfoliation of Graphite into Graphene in Aqueous Solutions of Inorganic Salts, *J. Am. Chem. Soc.*, 2014. vol. 136, p. 6083.
19. Sahoo, S.K. and Mallik, A., Simple, Fast and Cost-E® ective Electrochemical Synthesis of Few Layer Graphene Nanosheets, *NANO*, 2015, vol. 10, Article Number 1550019.
20. Paredes, J.I., Villar-Rodil, S., Solıs-Fernandez, P., Martınez-Alonso, A., and Tascon, J.M.D., Atomic Force and Scanning Tunneling Microscopy Imaging of Graphene Nanosheets Derived from Graphite Oxide, *Langmuir*, 2009, vol. 25, p. 5957.
21. Munuera, J.M., Paredes, J.I., Villar-Rodil, S., Ayán-Varela, M., Martínez-Alonso, A., and Tascón, J.M.D., Electrolytic exfoliation of graphite in water with multifunctional electrolytes: en route towards high quality, oxide–free graphene flakes, *Nanoscale*, 2016, vol. 8, p. 2982.
22. Shirley, D.A., Hyperfine Interactions and ESCA Data, *Phys. Scripta.*, 1975, vol. 11, P. 117.
23. Stankovich, S., Dikin, D.A., Piner, R.D., Kohlhaas, K.A., Kleinhammes, A., Jia, Y., Wu, Y., Nguyen, S.T., and Ruoff, R.S., Synthesis of graphene-based nanosheets via chemical reduction of exfoliated graphite oxide, *Carbon*, 2007, vol. 45, p. 1558.
24. Shulga, Y.M., Baskakov, S.A., Knerelman, E.I., Davidova, G.I., Badamshina, E.R., Shulga, N.Yu., Skryleva, E.A., Agapov, A.L., Voylov, D.N., Sokolov, A.P., and Martynenko, V.M., Carbon nanomaterial produced by microwave exfoliation of graphite oxide: new insights, *RSC Adv.*, 2014, vol. 4, p. 587.
25. Brownson, D.A.C., Foster, C.W., and Banks, C.E., The electrochemical performance of graphene modified electrodes: An analytical perspective, *Analyst.*, 2012, vol. 137, p. 1815.
26. Beidaghi, M., Wang, Z., Gu, L., and Wang, C., Electrostatic spray deposition of graphene nanoplatelets for high-power thin-film supercapacitor electrodes, *J. Solid State Electrochem.*, 2012, vol. 16, p. 3341.
27. Carter, R., Oakes, L., Cohn, A., Holzgrafe, J., Zarick, H.F., Chatterjee, S., Bardhan, R., and Pint, C.L., Solution Assembled Single Walled Carbon Nanotube Foams; Superior Performance in Supercapacitors, Lithium Ion, and Lithium Air Batteries, *J. Phys. Chem. C*, 2014, vol. 118, p. 20137.
28. Komarova, N.S., Krivenko, A.G., Ryabenko, A.G., and Naumkin, A.V., Active forms of oxygen as agents for electrochemical functionalization of SWCNTs, *Carbon*, 2013, vol. 53, p. 188.
29. Yamada, Y., Kimizuka, O., Tanaike, O., Machida, K., Suematsu, S., Tamamitsu, K., Saeki, S., Yoshizawa, N., Yamashita, J., Don, F., Hata, K., and Hatori, H., Capacitor Properties and Pore Structure of Single- and Double-Walled Carbon Nanotubes, *Electrochem. Solid-State Lett.*, 2009, vol. 12, K14–K16.
30. Krivenko, A.G., Komarova, N.S., Stenina, E.V., Sviridova, L.N., Mironovich, K.V., Shul'ga, Yu.M., Manzhos, P.A., Doronin, S.V., and Krivchenko, V.A., Electrochemical Modification of Electrodes Based on Highly Oriented Carbon Nanowalls, *Russ. J. Electrochem.*, 2015, vol. 51, p. 963.
31. Valota, A.T., Kinloch, I.A., Novoselov, K.S., Casiraghi, C., Eckmann, A., Hill, E.W., and Dryfe, R.A.W., Electrochemical Behavior of Monolayer and Bilayer Graphene, *ACS NANO*, 2012, vol. 5, p. 8809.
32. Oldham, K.B. and Myland, J.C., Modelling cyclic voltammetry without digital simulation, *Electrochim. Acta*, 2011, vol. 56, p. 10612.
33. Komarova, N.S., Krivenko, A.G., Stenina, E.V., Sviridova, L.N., Mironovich, K.V., Shulga, Y.M., and Krivchenko, V.A., Enhancement of the Carbon Nanowall Film Capacitance. Electron Transfer Kinetics on Functionalized Surfaces, *Langmuir*, 2015, vol. 31, p. 7129.
34. Komarova, N.S., Krivenko, A.G., Ryabenko, A.G., Naumkin, A.V., Maslakov, K.I., and Savilov, S.V.,

Functionalization and defunctionalization of single walled carbon nanotubes: Electrochemical and morphologic consequences, *J. Electroanal. Chem.*, 2015, vol. 738, p. 27.

35. Ambrosi, A. and Pumera, M., Electrochemistry at CVD Grown Multilayer Graphene Transferred onto Flexible Substrates, *J. Phys. Chem. C*, 2013, vol. 117, p. 2053.
36. Hong, C., Wong, A., Ambrosi, A., and Pumera, M., Thermally reduced graphenes exhibiting a close relationship to amorphous carbon, *Nanoscale*, 2012, vol. 4, p. 4972.
37. Punckt, C., Pope, M.A., and Aksay, I.A., High Selectivity of Porous Graphene Electrodes Solely Due to Transport and Pore Depletion Effects, *J. Phys. Chem. C*, 2014, vol. 118, p. 22635.
38. Cai, M., Outlaw, R.A., Butler, S.M., and Miller, J.R., A high density of vertically-oriented graphenes for use in electric double layer capacitors, *Carbon*, 2012, vol. 50, p. 5481.
39. Zhang, F., Lu, L., Yang, M., Gao, C., and Wang, Z., Electrochemistry of Graphene Flake Electrodes: Edge and Basal Plane Effect for Biosensing, *Int. J. Electrochem. Sci.*, 2016, vol. 11, p. 10172.
40. Brownson, D.A.C., Varey, S.A., Hussain, F., Haigh, S.J., and Banks, C.E., Electrochemical properties of CVD grown pristine graphene: monolayer- vs. quasi-graphene, *Nanoscale*, 2014, vol. 6, p. 1607.
41. Regisser, F., Lavoie, M.-A., Champagne, G.Y., and Belanger, D., Randomly oriented graphite electrode. Part 1. Effect of electrochemical pretreatment on the electrochemical behavior and chemical composition of the electrode, *J. Electroanal. Chem.*, 1996, vol. 415, p. 47.

Translated by Yu. Pleskov